NJC

PAPER

View Article Online
View Journal | View Issue

Cite this: *New J. Chem.*, 2015, 39, 6642

CO oxidation over Cu_2O deposited on 2D continuous lamellar g-C_3N_4

Yukun Shi, Xiaojing Hu, Jingtao Zhao, Xiaojiao Zhou, Baolin Zhu, Shoumin Zhang and Weiping Huang*

Received (in Porto Alegre, Brazil) 13th March 2015,
Accepted 2nd July 2015

DOI: 10.1039/c5nj00621j

www.rsc.org/njc

Cu_2O deposited on 2D continuous lamellar g-C_3N_4 (Cu_2O/g-C_3N_4) was prepared *via* a facile impregnation–chemical reduction procedure. The composition, structure and morphology of as-prepared Cu_2O/g-C_3N_4 were characterized by XRD, SEM, TEM, CO-TPR, FT-IR and nitrogen adsorption, respectively. The influence of Cu_2O loading on the performances of Cu_2O/g-C_3N_4, *e.g.* adsorption ability for methyl orange (MO) and the stability as well as catalytic activity for CO oxidation, was investigated. The changing trend of adsorption ability and the catalytic activity of Cu_2O/g-C_3N_4 moved in the same direction. When the mass ratio of Cu_2O to g-C_3N_4 was 4 : 10, the as-prepared composite exhibited the strongest adsorption ability and the highest catalytic activity; it also showed excellent stability in CO oxidation and over it the 100% conversion of CO was kept for more than 12 h under reaction conditions. The strong adsorption ability and good catalytic performance of Cu_2O/g-C_3N_4 were ascribed to the synergetic effects between g-C_3N_4 and Cu_2O as well as the improved dispersibility and the decreased particle size of Cu_2O.

Introduction

The catalytic oxidation of CO is an important reaction from the point of view of environmental protection and many other potential applications, such as automotive exhaust control and the operation of fuel cells.[1,2] For a long time, precious metals, *e.g.* Au,[3–5] Pt[6] and Pd[7], have been used for this reaction. However, the high cost and sensitivity to sulfur poisoning of precious metals prohibit their widespread exploitation in this reaction.[8] Researchers make a great effort to develop low-cost, high-activity modified and non-noble metal-based catalysts.[9] A copper-based catalyst is one of non-noble metal-based catalysts, being widely investigated for CO oxidation.[10–12] The Cu–Cu_2O–CuO system has been known to facilitate oxidation reactions in the bulk, suggesting that it has potential as a cost-effective substitute for noble metals in CO oxidation catalytic systems.[13] The CO oxidation rates over polycrystalline Cu, Cu_2O, and CuO, respectively, were investigated and the results showed that the reaction rate over Cu_2O was the highest,[14,15] which means that Cu_2O or supported Cu_2O for CO oxidation should be paid close attention and investigated in detail.

Generally, the supported catalysts for CO oxidation are alumina,[16,17] silica,[18] ceria,[1,8,19] and titanium oxide[3,5,20–22] supported ones. It has been extensively reported that the nature of the support affects enormously the catalytic activity of catalysts.[23,24] Catalysts are usually desired to finely disperse active species on a support with a high surface area for the efficient use of catalytically active components, which enhances the active area relative to the volume of catalysts and reduces the consumption and cost.[25] Therefore, many efforts have been made to develop new supports that are capable of developing suitable interactions with the loaded metal.[26–28]

Graphitic carbon nitride (g-C_3N_4), a superior catalyst support with high surface area, superior chemistry stability, amenability to chemical modification and many other fascinating properties, has been recently focused on heterogeneous catalysis.[29–31] As the s-triazine ring (C_3N_4) is aromatic, it is expected that a conjugated, two-dimensional polymer of s-triazine would tend to form a delocalized conjugated π structure like that of graphite.[32] Wang *et al.*[33] have reported that the delocalized conjugated π structure can interact with various metals, double- and triple-bond reactants, *e.g.* CO and so on, which should be favorable for reactions related to CO, *e.g.* CO oxidation. The delocalized conjugated π structure of g-C_3N_4 is also beneficial for improving electron transfer in the supported catalyst, which can play an important role in improving the stability of the highly dispersed metal particles. In particular, g-C_3N_4 with a large number of nitrogen atoms in the networks can stabilize metal particles by tight coordination. In the present contribution, we present a comprehensive study on CO oxidation over Cu_2O/g-C_3N_4 prepared *via* a facile impregnation-chemical reduction procedure and explore the relationship between adsorption ability and the catalytic activity of Cu_2O/g-C_3N_4.

College of Chemistry, Collaborative Innovation Center of Chemical Science and Engineering (Tianjin), The Key Laboratory of Advanced Energy Materials Chemistry (Ministry of Education) and Tianjin Key Lab of Metal and Molecule-based Material Chemistry, Nankai University, Tianjin 300071, China.
E-mail: hwp914@nankai.edu.cn; Tel: +86-13820096974

Experimental

Materials

All the reagents were of analytical grade and used without any further purification.

Preparation

g-C_3N_4. g-C_3N_4 was synthesized from urea by a facile template-free method.[34] In detail, 20.0 g of urea powder was put into a crucible with a cover, then the crucible was heated to 550 °C at a heating rate of 10 °C min^{-1} and kept for 2 h in a muffle furnace. The resultant yellow powder was collected for use without further treatment.

Cu_2O. The calculated amounts of cupric nitrate were dissolved in distilled water (50 mL) to form a solution. Then, NaOH aqueous solution (0.2 mol L^{-1}) and ascorbic acid aqueous solution (0.1 mol L^{-1}) were added dropwise, while being vigorously stirred, into the cupric nitrate solution, respectively. After addition, the mixture was continually stirred for another 4 h at 50 °C to form a claybank precipitation. The precipitate of Cu_2O was filtered, and washed several times with distilled water and ethanol, and dried at 40 °C in a vacuum for 12 h.

Cu_2O/g-C_3N_4. Cu_2O/g-C_3N_4 was synthesized *via* the following typical procedure. The calculated amounts of cupric nitrate were dissolved in distilled water (50 mL) to form a solution, and g-C_3N_4 (0.5 g) was added to the solution, and the mixture was vigorously stirred for 1 h. After low-energy sonication for 0.5 h, the NaOH aqueous solution (0.2 mol L^{-1}) and ascorbic acid aqueous solution (0.1 mol L^{-1}) were added dropwise, while being vigorously stirred, into the mixture, respectively. After addition, the mixture was continually stirred for another 4 h at 50 °C. Finally, the precipitate of Cu_2O/g-C_3N_4 was filtered, and washed to neutral with distilled water and ethanol, and dried at 40 °C in a vacuum for 12 h. The samples with various mass ratios of Cu_2O to g-C_3N_4, 2 : 10, 3 : 10, 4 : 10, 5 : 10 and 6 : 10, were marked as Cu_2O/g-C_3N_4-2, Cu_2O/g-C_3N_4-3, Cu_2O/g-C_3N_4-4, Cu_2O/g-C_3N_4-5 and Cu_2O/g-C_3N_4-6, respectively.

Catalyst characterization

TEM images of Cu_2O and Cu_2O/g-C_3N_4 were obtained using a JEM-2100 TEM working at 200 kV. The surface morphologies of Cu_2O and Cu_2O/g-C_3N_4 were observed using an X-650 scanning electron microscope (SEM) operating at 25 kV. The powder XRD experiments were carried out at room temperature using a Rigaku D/Max-2500 X-ray diffractometer (CuKa λ = 0.154 nm) to identify the crystal phase of the samples. FT-IR spectra were recorded on a Fourier transform infrared spectrometer (Bruker Vector 22). The specific surface areas (SSA) were measured by nitrogen adsorption (BET, JW-K, at liquid N_2 temperature).

Temperature-programmed reduction with CO (CO-TPR) experiment was carried out using a Micromeritics TPR 2910 instrument. The sample (0.05 g) was loaded in a quartz tube reactor and flushed with Ar at 120 °C for 60 min. Then CO-TPR was performed by heating the samples to 800 °C at a ramp rate of 10 °C min^{-1} in a flow of 10% CO/Ar mixture with a rate of 30 mL min^{-1}. TCD was used to detect new gas formed in the determination process.

Catalytic tests

The absorption abilities of as-prepared Cu_2O, g-C_3N_4 and Cu_2O/g-C_3N_4 were measured by their decoloration activities for MO solution in the dark. Typically, catalyst (0.05 g) and 60 mL of MO aqueous solution (20 mg L^{-1}, neutral) were put into a 60 mL quartz test tube. The tube was placed in a dark box with magnetic stirring. At regular time intervals, a sample of mixture was withdrawn and centrifuged, and the MO concentration of clear solution was measured using a TU-1901 UV-vis spectrometer at 463.8 nm, which is the maximum absorption wavelength of MO.

The evaluation of catalytic activities of Cu_2O and Cu_2O/g-C_3N_4 for CO oxidation was carried out in a fixed-bed flow microreactor under atmospheric pressure using 200 mg Cu_2O or Cu_2O/g-C_3N_4 samples containing 200 mg Cu_2O. A stainless steel tube with an inner diameter of 8 mm was chosen as the reactor tube. The catalyst was diluted with chemically inert quartz sand. The reaction gas mixture consisting of 10% CO balanced with air was passed through the catalyst bed at a total flow rate of 36.3 mL min^{-1}. The temperature dependence of the sample catalytic activity was recorded in the range of 100–220 °C at a ramping rate of 10 °C min^{-1}. After holding at the reaction temperature for 30 min, effluent gases were analyzed on-line by GC-508A gas chromatography. The activity was expressed by the degree of conversion of CO.

Results and discussion

Structure and morphology

The morphology of g-C_3N_4 was clearly visualized using a transmission electron microscope (TEM), as shown in Fig. 1a. The synthesized g-C_3N_4 shows an obvious two-dimensional (2D) continuous lamellar structure, which is consistent with that reported in the previous report.[32] The enlarged view in Fig. 1a indicates that the edges of the layers tend to bend in order to reduce surface energy.[34] The XRD pattern shown in Fig. 1b displays two pronounced diffraction peaks of (100) and (002) planes at 2θ = 13.1° and 27.1°, which can be ascribed to the characteristic inter-layer structural packing and the interplanar stacking peaks of the aromatic systems, respectively. Fig. 1c depicts the FTIR spectra of g-C_3N_4. A broad band centered at 3188 cm^{-1} corresponds to the stretching modes of terminal NH groups at the defect sites of the aromatic ring. The absorption band at 1641 cm^{-1} can be ascribed to the C–N stretching vibration modes, while the four strong peaks at 1253, 1329, 1417 and 1572 cm^{-1} to the CN heterocycle stretching of g-C_3N_4. The absorption band at 808 cm^{-1} can be assigned to breathing mode of the heptazine ring system. These are consistent with the reported values. These results indicate that g-C_3N_4 has been synthesized.

Fig. 2 shows the XRD patterns of Cu_2O and Cu_2O/g-C_3N_4 with different mass ratios. As can be seen, all samples show the diffraction peaks at 29.6°, 36.4°, 42.3°, 61.5°, 73.6° and 77.5°,

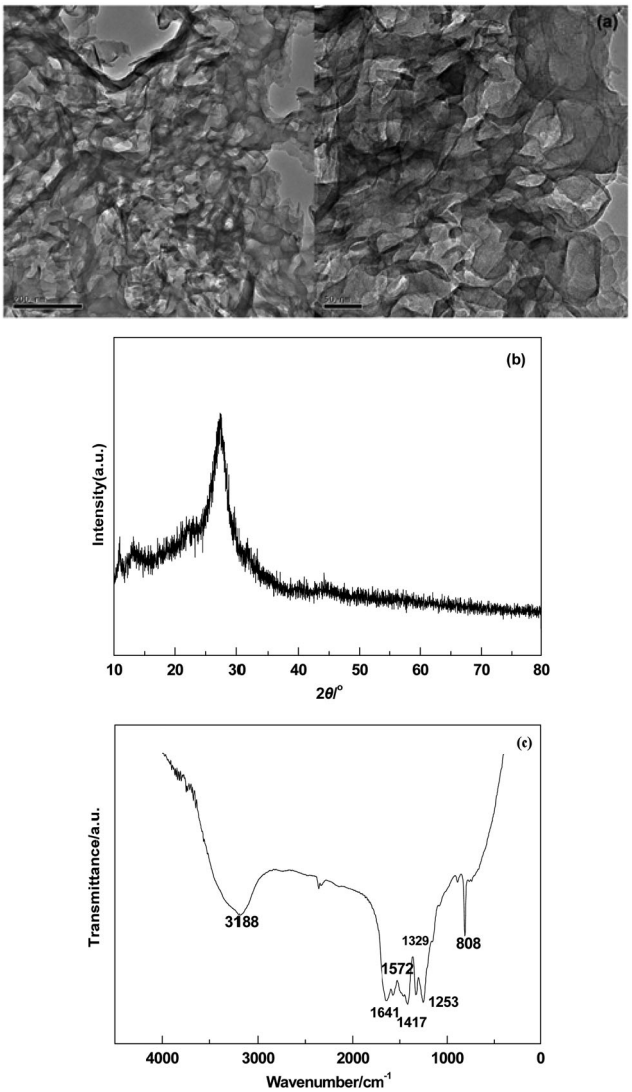

Fig. 1 TEM images (a), XRD pattern (b) and FT-IR pattern (c) of g-C_3N_4.

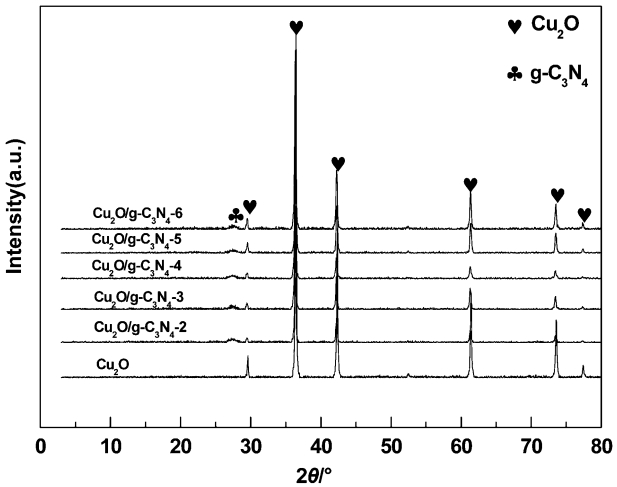

Fig. 2 XRD patterns of Cu_2O and Cu_2O/g-C_3N_4 with different mass ratios.

Table 1 SSA of Cu_2O, g-C_3N_4 and Cu_2O/g-C_3N_4 with different mass ratios

Samples	Cu_2O	g-C_3N_4	Cu_2O/ g-C_3N_4-2	Cu_2O/ g-C_3N_4-3	Cu_2O/ g-C_3N_4-4	Cu_2O/ g-C_3N_4-5
S_{BET} (m^2 g^{-1})	0.9	293	76	71	65	37

which can be attributed to the (110), (111), (200), (220), (311) and (222) planes of cubic Cu_2O, corresponding to JCPDS card no. 65-3288. No obvious peaks corresponding to CuO or Cu are observed in the patterns. Compared with that of Cu_2O, the patterns of Cu_2O/g-C_3N_4 samples have no obvious difference, indicating that the existence of g-C_3N_4 does not change the crystal form of Cu_2O. It is noteworthy that for Cu_2O and Cu_2O/g-C_3N_4 samples, the (111) diffraction peaks of Cu_2O are all the strongest, which implies that {111} facets are dominated in samples. In the XRD patterns of Cu_2O/g-C_3N_4, the weak peak related to g-C_3N_4 (002) appears at 27.1°, indicating that g-C_3N_4 and cubic Cu_2O phases coexist in the composite.

The SSA of Cu_2O, g-C_3N_4 and Cu_2O/g-C_3N_4 with different mass ratios are listed in Table 1. The SSA of primary Cu_2O and g-C_3N_4 are 0.9 and 293 m^2 g^{-1}, respectively; the latter is consistent with the relevant literature of g-C_3N_4.[34] The SSA of all Cu_2O/g-C_3N_4 samples are lower than that of pure g-C_3N_4, and decrease with the increase of Cu_2O content. It can be envisioned that the high surface area of g-C_3N_4 should be able to improve the dispersibility and decrease the particle size of Cu_2O.

The morphologies and detailed microstructure of as-prepared Cu_2O particles and Cu_2O/g-C_3N_4-4 were investigated by SEM and HRSEM analyses. It can be seen from Fig. 3a that most particles of as-prepared Cu_2O are octahedral and their size is about 400–700 nm, which is in accordance with the relevant results of literature.[35,36] The SEM images of Cu_2O/g-C_3N_4-4 shown in Fig. 3b and c clearly display that the sample is composed of Cu_2O particles and g-C_3N_4, in which the size of the Cu_2O particle is smaller than that of prime Cu_2O (Fig. 3a) and there is a close interface between Cu_2O and g-C_3N_4, which obviously demonstrates that the smaller Cu_2O particles can be separated from each other by g-C_3N_4 efficiently. It is understandable that the two-dimensional (2D) continuous lamellar structure of g-C_3N_4 with delocalized conjugated π-bonds can offer plentiful of nucleation sites and N-donor ligands, preventing Cu_2O particles from aggregation leading to the formation of discrete Cu_2O particles,[37] which should be beneficial for enhancing the catalytic activity for CO oxidation.

Fig. 4 shows the TEM images of Cu_2O/g-C_3N_4-4. As shown in Fig. 4a, Cu_2O/g-C_3N_4-4 with particle-on-sheet morphology is obtained; all Cu_2O particles are deposited or attached to the surface of the g-C_3N_4 substrate and the size of Cu_2O particles is 100–200 nm, which is smaller than that of pure Cu_2O. The HRTEM image of the as-prepared Cu_2O/g-C_3N_4-4 also clearly reveals a close interface between Cu_2O and g-C_3N_4 in the as-prepared composite, which is significant for electron transfer between the Cu_2O and g-C_3N_4 layer.[38]

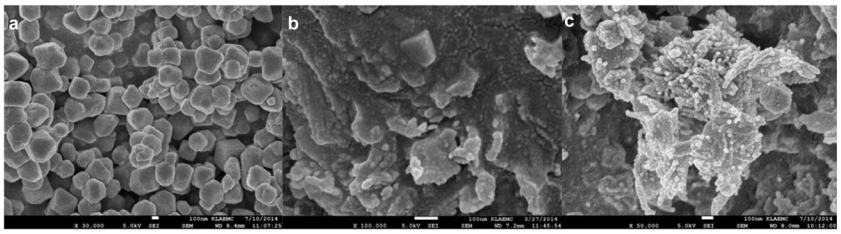

Fig. 3 SEM images of Cu_2O (a) and $Cu_2O/g\text{-}C_3N_4$-4 (b and c).

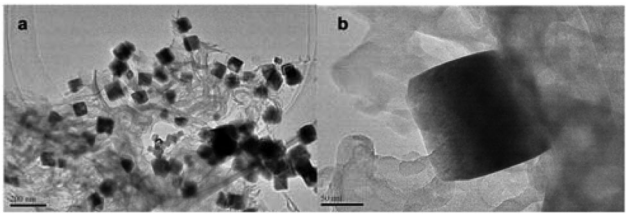

Fig. 4 TEM images of $Cu_2O/g\text{-}C_3N_4$-4.

CO-TPR analysis

The oxidisability and stability of the $Cu_2O/g\text{-}C_3N_4$ composite in CO were studied by means of CO-TPR, and the results are shown in Fig. 5. For $g\text{-}C_3N_4$, its CO-TPR is actually a temperature programmed decomposition because $g\text{-}C_3N_4$ is not reducible with CO + Ar. As shown in Fig. 5, $g\text{-}C_3N_4$ shows a distinguished peak at around 700 °C, which is ascribed to the thermal vaporization and decomposition of $g\text{-}C_3N_4$. Wang *et al.*[33] have reported that the sublimation of $g\text{-}C_3N_4$ increased massively at 650 °C and complete decomposition occurred at 750 °C. Compared with $g\text{-}C_3N_4$, $Cu_2O/g\text{-}C_3N_4$-4 shows two CO reduction peaks centered at 420 and 630 °C, corresponding to the reduction of various Cu_2O crystals on $g\text{-}C_3N_4$. Fig. 5 clearly reveals that $Cu_2O/g\text{-}C_3N_4$ is stable and cannot be reduced by CO + Ar at temperature below 350 °C.

Adsorption ability

In order to explore the synergistic effect between $g\text{-}C_3N_4$ and Cu_2O in the as-prepared $Cu_2O/g\text{-}C_3N_4$ composite, the decoloration activities of samples for MO solution in the dark were characterized and the results are shown in Fig. 6. MO is a sulfonic acid sodium salt, which can clearly indicate the adsorption ability of the sample for negatively charged species in neutral solution. $g\text{-}C_3N_4$ has hardly any adsorption ability for MO within 1.5 h. However, the Cu_2O particles and $Cu_2O/g\text{-}C_3N_4$ show strong adsorption for MO under the same conditions. Moreover, $Cu_2O/g\text{-}C_3N_4$-3 and $Cu_2O/g\text{-}C_3N_4$-4 show stronger adsorption ability than pure Cu_2O. This result strongly suggests that the intimate junctions between $g\text{-}C_3N_4$ and Cu_2O bring some synergistic effects to enhance the decoloration activity, or adsorption ability, of the $g\text{-}C_3N_4/Cu_2O$ composite. As the result of XRD, the {111} facets in Cu_2O particles are dominated, which is responsible for the strong adsorption ability of the Cu_2O particles. It is well known that the Cu_2O crystals bound by the {111} facets contain positively charged copper atoms on the surfaces,[39] which can interact more strongly with MO anions. This phenomenon should be noteworthy, because it suggests that the as-prepared $Cu_2O/g\text{-}C_3N_4$ may strongly interact between $g\text{-}C_3N_4$ and Cu_2O to enhance the catalytic activity of $Cu_2O/g\text{-}C_3N_4$ for CO oxidation. In addition, Cu_2O content can obviously affect the decoloration activity; $Cu_2O/g\text{-}C_3N_4$-4 displays the highest decoloration activity. It could be predicted that $Cu_2O/g\text{-}C_3N_4$-4 should also have the highest catalytic activity for CO oxidation.

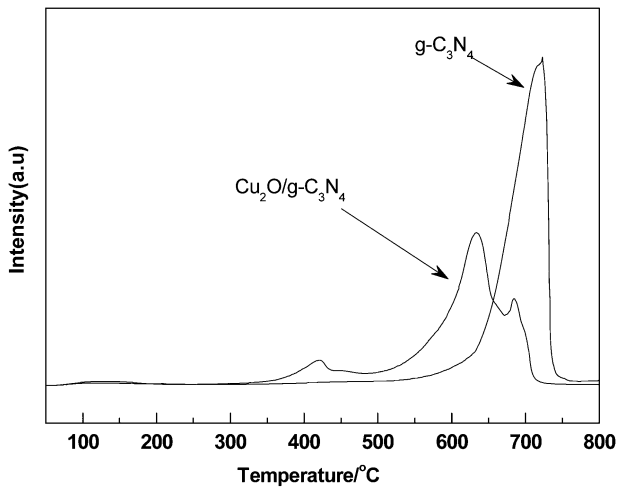

Fig. 5 CO-TPR profiles of $g\text{-}C_3N_4$ and $Cu_2O/g\text{-}C_3N_4$-4.

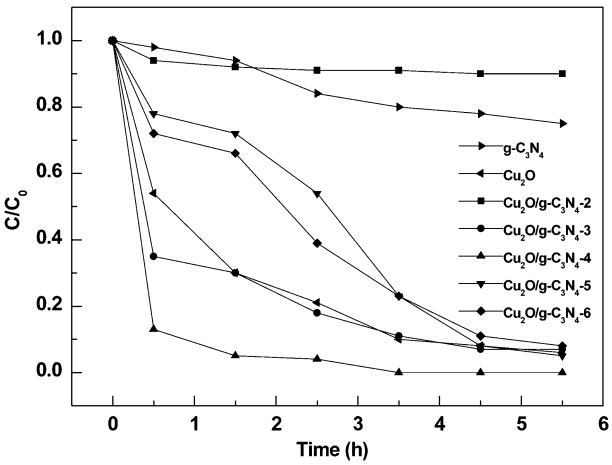

Fig. 6 Adsorption abilities of as-prepared $g\text{-}C_3N_4$, Cu_2O and $Cu_2O/g\text{-}C_3N_4$ for MO in the dark.

CO oxidation activity

The catalytic activities of Cu_2O and $Cu_2O/g\text{-}C_3N_4$ with different mass ratios for CO oxidation are shown in Fig. 7. It can be seen

from the figure that no significant CO conversion over the pure Cu_2O is found until 180 °C, and $T_{100\%}$ appears at about 220 °C. However, Cu_2O/g-C_3N_4 shows extremely attractive catalytic activity and the activity increases from Cu_2O/g-C_3N_4-2 to Cu_2O/g-C_3N_4-4; when the mass ratio of Cu_2O to g-C_3N_4 increases any further, the activity decreases (Cu_2O/g-C_3N_4-5). The high activities of the Cu_2O/g-C_3N_4 samples should come from synergetic effects of g-C_3N_4 and Cu_2O. Additionally, the improved dispersibility and the decreased particle size of Cu_2O of the as-prepared composites also play important roles in enhancing CO oxidation activity. Xu *et al.*[40] have reported that the {111} facets of Cu_2O have high surface atomic density of Cu atoms, which can provide more adsorbed and reactive sites; the two-dimensional (2D) continuous lamellar structure of g-C_3N_4 with high SSA can disperse Cu_2O particles so efficiently that more small Cu_2O particles form and increase in turn active sites for the oxidation reaction. It is obvious that Cu_2O/g-C_3N_4-4 exhibits the best catalytic performance, over which the CO oxidation starts at ~140 °C and 100% CO conversion can be achieved at ~200 °C with a T_{50} of ~180 °C. In comparison with Cu_2O/g-C_3N_4-4, the catalytic performance of Cu_2O/g-C_3N_4-5 decreases sharply. The result may be attributed to the fact that the high content of Cu_2O is not beneficial for dispersion of Cu_2O particles, which decreases the synergistic effects, *e.g.* the transfer of electrons between coordination unsaturated Cu of Cu_2O and g-C_3N_4.

The long-term stability of Cu_2O/g-C_3N_4 catalysts in the catalytic reaction is an important parameter to consider when evaluating the catalytic performance. The stability of Cu_2O/g-C_3N_4-4 was examined by running for 12 h and the results are presented in Fig. 8. After continuous operation for 12 h, the conversion of CO remains at 100% and no deactivation is found at 200 °C, indicating that the as-prepared Cu_2O/g-C_3N_4 catalysts have high stability for CO oxidation. In order to further confirm the stability of the Cu_2O/g-C_3N_4 catalysts, Cu_2O/g-C_3N_4-4 used for 12 h was collected and analyzed by XRD, which is shown in Fig. 9. It can be seen from Fig. 9 that the diffraction peaks assigned to Cu_2O match very well with JCPDS card no. 65–3288

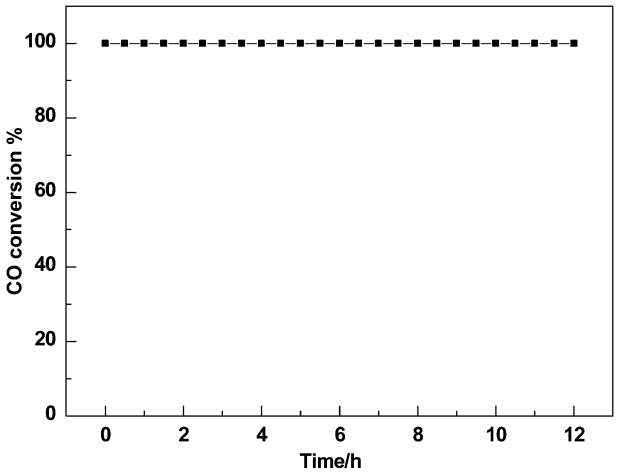

Fig. 8 Stability of Cu_2O/g-C_3N_4-4; reaction temperature: 200 °C.

and no peaks related to Cu or CuO are observed, which is in good agreement with the results of CO-TPR, indicating that no new species is generated in the process of CO oxidation. It can be concluded that the Cu_2O/g-C_3N_4 catalysts in the present contribution are highly stable based on the all results above.

Mechanism of CO oxidation

The interactions between Cu_2O and g-C_3N_4 are responsible for the results discussed above. Zhang *et al.* have reported the interactions between Pd atoms and g-C_3N_4.[38] The g-C_3N_4 has a lot of π orbitals, which can adjust the electron density of Cu_2O through the Pπ–dπ bonding between the π-orbitals of g-C_3N_4 and d-orbitals of coordination unsaturated Cu of Cu_2O. With the help of delocalization of electrons in the whole of Cu_2O/g-C_3N_4, the coordination unsaturated Cu of Cu_2O could accept the donation of CO + O_2 more effectively and enhance the catalytic activity of catalysts.

The reaction mechanism of CO oxidation over metal oxide catalyst has been well established.[8] It has been reported that

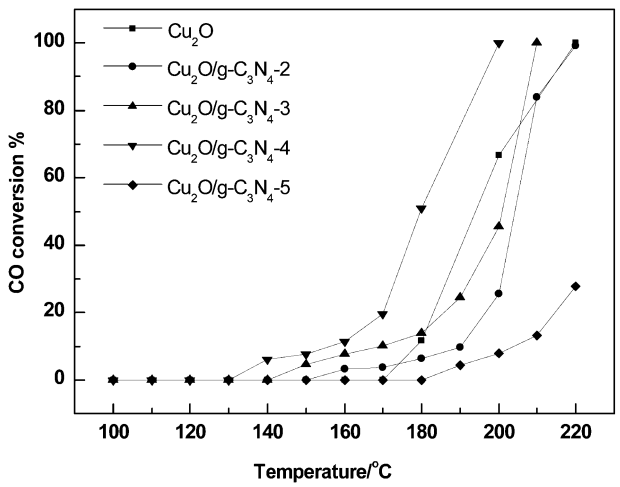

Fig. 7 Catalytic activities of Cu_2O and Cu_2O/g-C_3N_4 with different mass ratios.

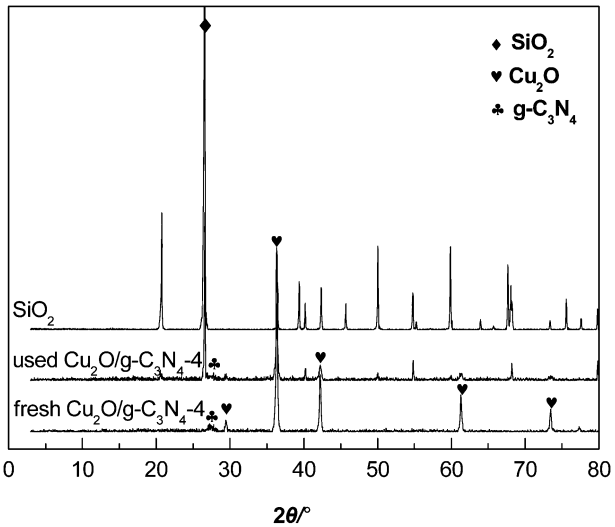

Fig. 9 XRD patterns of fresh Cu_2O/g-C_3N_4-4, used Cu_2O/g-C_3N_4-4 and SiO_2.

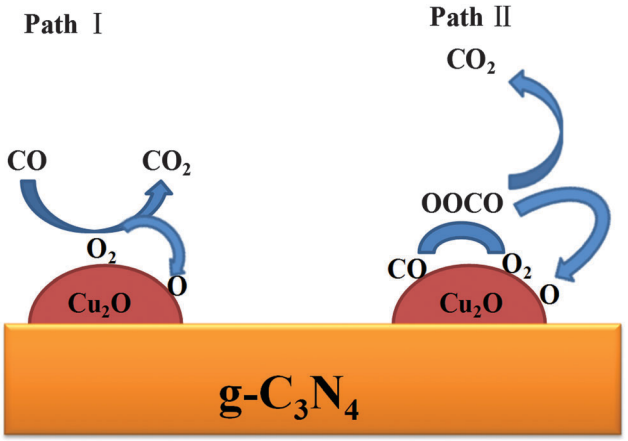

Scheme 1 The possible mechanism of $Cu_2O/g\text{-}C_3N_4$ catalysts for CO oxidation reaction.

Cu_2O has extremely high activation energy of 600 kJ mol^{-1}, which could be due to the extra energy needed to dissociate O_2 on the Cu_2O surface. Thus, the usual MVK mechanism is not suitable for CO oxidation on Cu_2O (111). Based on the relevant literature[9,41,42] and the results above, the mechanism of $Cu_2O/g\text{-}C_3N_4$ catalysts for CO oxidation reaction is proposed and shown in Scheme 1. The reaction could take place *via* two paths. Path I is that CO attacks the O_2 binding to Cu_2O to directly produce CO_2, which leaves behind an oxygen atom binding to the Cu_2O surface, namely, $CO_{(gas)} + O_{2(ads)} \rightarrow CO_{2(gas)} + O_{(ads)}$. Path II is of Langmuir–Hinshelwood type where adsorbed CO reacts with adsorbed oxygen. The peroxo-type (OOCO) complex generated from the co-adsorption of CO and O_2 decomposes into product CO_2, and an oxygen atom binding to the Cu_2O surface is left behind, namely, $CO_{(ads)} + O_{2(ads)} \rightarrow OOCO_{(ads)} \rightarrow CO_{2(gas)} + O_{(ads)}$.

Conclusions

In this paper, the Cu_2O deposited on 2D continuous lamellar $g\text{-}C_3N_4$ catalysts with different mass ratios were prepared *via* an impregnation–facile chemical reduction method. Cu_2O particles were highly dispersed on the surface and interspace of $g\text{-}C_3N_4$. The mass ratio of Cu_2O to $g\text{-}C_3N_4$ showed a significant influence on the adsorption ability and catalytic performance for CO oxidation. Cu_2O deposited on $g\text{-}C_3N_4$ with the mass ratio of 4 : 10 exhibited the strongest adsorption ability for methyl orange and the highest catalytic activity. The strong adsorption ability was ascribed to the dominant exposure of {111} facets in Cu_2O particles, which have the dangling bonds from the surface copper atoms interacting well with negative charged methyl orange. The enhancement of catalytic performance could be attributed to the synergetic effects between $g\text{-}C_3N_4$ and Cu_2O and the improved dispersibility of Cu_2O particles.

Acknowledgements

This work is supported by the National Natural Science Foundation of China (21373120, 21301098, 21071086 and 21271110), MOE Innovation Team (IRT13022) of China, and the Applied Basic Research Programs of Science and Technology Commission Foundation of Tianjin (13JCQNJC02000 and 12JCYBJC13100).

References

1 F. Yang, J. Graciani, J. Evans, P. Liu, J. Hrbek, J. Fdez. Sanz and J. A. Rodriguez, *J. Am. Chem. Soc.*, 2011, **133**, 3444.
2 K. N. Rao, P. Bharali, G. Thrimurthulu and B. Reddy, *Catal. Commun.*, 2010, **11**, 863.
3 H. Zhao, P. Zhang, Y. D. Wang, W. P. Huang and S. M. Zhang, *J. Sol–Gel Sci. Technol.*, 2014, **71**, 406.
4 J. A. Rodrigueza, R. Si, J. Evans, W. Q. Xu, J. C. Hanson, J. Tao and Y. M. Zhu, *Catal. Today*, 2015, **240**, 229.
5 Y. L. Chen, B. L. Zhu, M. Y. Yao, S. R. Wang and S. M. Zhang, *Catal. Commun.*, 2010, **11**, 1003.
6 M. Q. Shen, L. F. Lv, J. Q. Wang, J. X. Zhu, Y. Huang and J. Wang, *Chem. Eng. J.*, 2014, **255**, 40.
7 S. Y. Wang, N. Li, R. M. Zhou, L. Y. Jin, G. S. Hu, J. Q. Lu and M. F. Luo, *J. Mol. Catal. A: Chem.*, 2010, **26**, 18113.
8 B. Z. Sun, W. K. Chen and Y. J. Xu, *J. Chem. Phys.*, 2010, **133**, 154502.
9 P. Zhang, J. L. Guo, P. Zhao, B. L. Zhu, W. P. Huang and S. M. Zhang, *RSC Adv.*, 2015, **5**, 11989.
10 A. Hornés, A. B. Hungría, P. Bera, A. López Cámara, M. Fernández-García, A. Martínez-Arias, L. Barrio, M. Estrella, G. Zhou, J. J. Fonseca, J. C. Hanson and J. A. Rodriguez, *J. Am. Chem. Soc.*, 2010, **132**, 34.
11 B. Solsona, G. J. Hutchings, T. Garcia and S. H. Taylor, *New J. Chem.*, 2004, **28**, 708.
12 Z. X. Yang, B. L. He, Z. S. Lu and K. Hermansson, *J. Phys. Chem. C*, 2010, **114**, 4486.
13 B. White, M. Yin, A. Hall, D. Le, S. Stolbov, T. Rahman, N. Turro and S. O'Brien, *Nano Lett.*, 2006, **6**, 2095.
14 T. J. Huang and D. H. Tsai, *Catal. Lett.*, 2003, **87**, 173.
15 B. Z. Sun, W. K. Chen and Y. J. Xu, *J. Chem. Phys.*, 2009, **131**, 174503.
16 N. Chotigkrai, J. Panpranot and P. Praserthdam, *Catal. Commun.*, 2014, **56**, 92.
17 Z. Boukha, J. L. Ayastuy, A. Iglesias-González, B. Pereda-Ayo, M. A. Gutiérrez-Ortiz and J. R. González-Velasco, *Appl. Catal., B*, 2014, **160–161**, 629.
18 M. I. Zaki, M. A. Hasan, L. Pasupulety, N. E. Fouad and H. Knozinger, *New J. Chem.*, 1999, **23**, 1197.
19 C. K. Krishnan, K. Nakamura, H. Hirata and M. Ogura, *Phys. Chem. Chem. Phys.*, 2010, **12**, 7513.
20 M. Y. Kang, H. J. Yun, S. Yu, W. Kim, N. D. Kim and J. Yi, *J. Mol. Catal. A: Chem.*, 2013, **368–369**, 72.
21 Y. C. Jiao, H. L. Jiang and F. Chen, *ACS Catal.*, 2014, **4**, 2249.
22 L. Li, Y. Gao, H. Li, Y. Zhao, Y. Pei, Z. F. Chen and X. C. Zeng, *J. Am. Chem. Soc.*, 2013, **135**, 19336.
23 N. Hammer, K. Mathisen and M. Rønning, *Top. Catal.*, 2013, **56**, 637.
24 D. Widmann and R. J. Behm, *Acc. Chem. Res.*, 2014, **47**, 740.

25 Y. N. Tang, Z. X. Yang, X. Q. Dai, Z. S. Lu, Y. X. Zhang and Z. M. Fu, *J. Nanosci. Nanotechnol.*, 2014, **14**, 7117.
26 W. L. Han, Z. C. Tang, P. Zhang, G. X. Lu and X. Pan, *Colloids Surf., A*, 2014, **460**, 422.
27 M. Scarisoreanu, R. Alexandrescu, I. Morjan, R. Birjega, C. Luculescu, E. Popovici, E. Dutu, E. Vasile, V. Danciu and N. Herlin-Boime, *Appl. Surf. Sci.*, 2013, **278**, 295.
28 S. K. Jain, E. M. Crabb, L. E. Smart, D. Thompsett and A. M. Steele, *Appl. Catal., B*, 2009, **89**, 349.
29 G. S. Wu, S. S. Thind, J. L. Wen, K. Yan and A. C. Chen, *Appl. Catal., B*, 2013, **142–143**, 590.
30 F. Chang, Y. C. Xie, C. L. Li, J. Chen, J. R. Luo, X. F. Hu and J. W. Shen, *Appl. Surf. Sci.*, 2013, **280**, 967.
31 M. Xu, L. Han and S. J. Dong, *ACS Appl. Mater. Interfaces*, 2013, **5**, 12533.
32 B. Chai, T. Y. Peng, J. Mao, K. Li and L. Zan, *Phys. Chem. Chem. Phys.*, 2012, **14**, 16745.
33 Y. Wang, X. C. Wang and M. Antonietti, *Angew. Chem., Int. Ed.*, 2012, **51**, 68.
34 F. Dong, Z. Y. Wang, Y. J. Sun, W. K. Ho and H. D. Zhang, *J. Colloid Interface Sci.*, 2013, **401**, 70.
35 X. J. Yu, Y. C. Wei, L. Z. Huang, J. F. Niu, J. Zhang, X. M. Li and B. H. Yao, *Mater. Chem. Phys.*, 2014, **148**, 727.
36 Q. Hua, T. Cao, H. Z. Bao, Z. Q. Jiang and W. X. Huang, *ChemSusChem*, 2013, **6**, 1966.
37 J. Zhang, W. X. Liu, X. W. Wang, X. Q. Wang, B. Hu and H. Liu, *Appl. Surf. Sci.*, 2013, **282**, 84.
38 W. Y. Zhang, H. J. Huang, F. Li, K. M. Deng and X. Wang, *J. Mater. Chem. A*, 2014, **2**, 19084.
39 J. Y. Ho and M. H. Huang, *J. Phys. Chem. C*, 2009, **113**, 14159.
40 Y. Xu, H. Wang, Y. F. Yu, L. Tian, W. W. Zhao and B. Zhang, *J. Phys. Chem. C*, 2011, **115**, 15288.
41 G. J. Wu, N. J. Guan and L. D. Li, *Catal. Sci. Technol.*, 2011, **1**, 601.
42 G. G. Jernigan and G. A. Somorjai, *J. Catal.*, 1994, **147**, 567.

